JGR Oceans

RESEARCH ARTICLE
10.1029/2024JC021425

A Link Between U.S. East Coast Sea Level and North Atlantic Subtropical Ocean Heat Content

Jacob M. Steinberg[1], Stephen M. Griffies[1,2], John P. Krasting[1], Christopher G. Piecuch[3], and Andrew C. Ross[1]

[1]NOAA Geophysical Fluid Dynamics Laboratory, Princeton, NJ, USA, [2]Princeton University Atmospheric and Oceanic Sciences Program, Princeton, NJ, USA, [3]Woods Hole Oceanographic Institution, Woods Hole, MA, USA

Key Points:

- A recently developed high-resolution regional ocean model faithfully reproduces the space-time structure of sea level change in this region
- Coastal sea level south of Cape Hatteras covaries with offshore mode water heat content
- Cross-shore ocean mass redistribution is correlated with offshore subsurface density change

Correspondence to:

J. M. Steinberg,
jacob.steinberg@noaa.gov

Citation:

Steinberg, J. M., Griffies, S. M., Krasting, J. P., Piecuch, C. G., & Ross, A. C. (2024). A Link between U.S. East coast sea level and North Atlantic subtropical ocean heat content. *Journal of Geophysical Research: Oceans*, *129*, e2024JC021425. https://doi.org/10.1029/2024JC021425

Received 4 JUN 2024
Accepted 21 NOV 2024

Author Contributions:

Conceptualization: Jacob M. Steinberg, Stephen M. Griffies
Data curation: Jacob M. Steinberg
Formal analysis: Jacob M. Steinberg, Andrew C. Ross
Investigation: Jacob M. Steinberg, Stephen M. Griffies, John P. Krasting, Christopher G. Piecuch
Methodology: Jacob M. Steinberg, Stephen M. Griffies, John P. Krasting, Christopher G. Piecuch
Resources: Jacob M. Steinberg
Software: Jacob M. Steinberg, Andrew C. Ross
Supervision: Stephen M. Griffies, John P. Krasting
Validation: Jacob M. Steinberg, Andrew C. Ross
Visualization: Jacob M. Steinberg

Abstract Using a recently developed 1/12th degree regional ocean model, we establish a link between U.S. East Coast sea level variability and offshore upper ocean heat content change. This link manifests as a cross-shore mass redistribution driven by an offshore thermosteric sea level response to subsurface warming or cooling. Approximately 50% of simulated monthly to interannual coastal sea level variance south of Cape Hatteras can be statistically accounted for by this mechanism, realized as a function of regional ocean hypsometry, gyre scale warming, and the depth dependence of density change. This response to offshore warming explains the nonstationarity of U.S. East Coast sea level covariance, a specifically observed and modeled behavior after ~2010. Since approximately 2010, elevated rates of sea level rise south of Cape Hatteras can be partly explained as the result of shoreward mass redistribution due to offshore subsurface warming within the North Atlantic subtropical gyre. These results reveal a mechanism that connects local coastal sea level to a broader region and identifies the influence of regional heat content changes on coastal sea level. This analysis presents a framework for identifying new regions that may be susceptible to enhanced sea level rise due to ocean warming and helps bridge the gap between quantifying large scale change and anticipating local coastal impacts that can make flooding and storm surge more acutely damaging.

Plain Language Summary In this work, we establish a link between subtropical North Atlantic Ocean heat content and coastal sea level south of Cape Hatteras, in the Caribbean Sea, and within the Gulf of Mexico. Using a newly developed high-resolution ocean simulation, coastal sea level is found to rise and fall in tandem with offshore upper ocean warming or cooling events. This connection is realized at seasonal and longer timescales and thus explains a baseline sea level change about which higher frequency storm and flooding events can cause damage. In this framework, approximately half of coastal sea level variability can be explained by seasonal to interannual offshore density change below the continental shelf break depth. This equilibrium coastal response both links coastal regions experiencing acute sea level rise to regions of ocean warming and reveals a mechanism that can be employed to anticipate future change.

1. Introduction

Tide gauge measurements of coastal sea level represent some of the longest persistent oceanographic records, some of which exceed 100 years in length (e.g., at Charleston, SC; Hogarth (2014); Talke et al. (2018)). Individually, these records reveal disparate patterns of regional sea level change across a range of timescales (Thompson & Mitchum, 2014; Woodworth et al., 2019), but together, show global mean sea level to be rising at an increasing rate (Frederikse et al., 2020). Over the past three decades, following the implementation of global observing systems (e.g., satellite altimetry, Argo, and GRACE), measurements of ocean heat content and mass change enable more detailed analyses of the patterns and drivers of sea level variability indirectly observed by tide gauges (Chen et al., 2019; Frederikse et al., 2020; Hamlington et al., 2022; Johnson & Lyman, 2020). At regional spatial and subdecadal temporal scales, however, disentangling underlying physical processes that drive observed changes is often difficult due to limited observational spatiotemporal resolution (Cazenave & Moreira, 2022). Global and regional ocean simulations offer a unique opportunity to directly consider these scale-dependent responses to oceanic heat and mass change, and importantly, to determine how these changes manifest at the coast. Recent improvements in model representation of sea level-related processes (Fox-Kemper et al., 2019; Griffies et al., 2014), including western boundary current and boundary layer dynamics, along with increases in horizontal resolution result in simulated sterodynamic variability that better match observations, especially near the coast (D. Li et al., 2022), and aligns with improvements in reanalysis products (Feng et al., 2024). These

Writing – original draft: Jacob M. Steinberg
Writing – review & editing: Jacob M. Steinberg, Stephen M. Griffies, John P. Krasting, Christopher G. Piecuch, Andrew C. Ross

improvements allow projected coastal flood risks to be more accurately detailed (Sun et al., 2023; Sweet et al., 2022, 2024) and tailored to impacted communities (Nicholls, 2015; Nicholls et al., 2021).

Many recent observation- and model-based studies have identified coastlines along the U.S. East Coast south of Cape Hatteras and within the Gulf of Mexico as a region experiencing rates of sea level rise greater than the global mean (e.g., Dangendorf et al. (2021); Harvey et al. (2021); Dangendorf et al. (2023); Yin (2023); Steinberg et al. (2024); Zhang et al. (2024)). Low-lying coastal areas in this region have been particularly impacted, which is partly the result of natural and anthropogenically driven land subsidence (Kolker et al., 2011; Liu et al., 2020), and also proximity to the Gulf Stream carrying warm equatorial waters poleward. South of Cape Hatteras, changes in Gulf Stream transport correspond to changes in the cross-shore sea level gradient such that a decrease in transport drives an increase in coastal sea level (Chi et al., 2023; Ezer & Dangendorf, 2020; Ezer et al., 2013). While interannual changes in transport have been linked more broadly to the Atlantic meridional overturning circulation (AMOC) and phases of the North Atlantic Oscillation (NAO), westward propagating eddies make correlations between transport and coastal sea level difficult to diagnose (Little et al., 2019). Shifts in the central latitude of the Gulf Stream extension have also been linked to heat content and coastal sea level variability (Dong et al., 2019; Ezer, 2019; Todd & Ren, 2023), with this position more directly related to basin-scale wind and buoyancy forcing associated with the NAO (Wang et al., 2022, 2024; Zhang et al., 2024).

Of the complex set of offshore physical processes that contribute to coastal sea level change in this region, the ocean's static equilibrium response to warming (Greatbatch, 1994; Domingues et al., 2018; Z. Li et al., 2023; Steinberg et al., 2024) remains underexplored. One component of this response has been realized as a shoreward redistribution of ocean mass resulting from offshore subsurface warming (Landerer et al., 2007; Steinberg et al., 2024). As changes in subtropical North Atlantic heat storage have been linked to coastal sea level change (Volkov et al., 2019, 2023), we hypothesize that this mechanism may be important and influencing coastal sea level rise. The nature of this response offers an opportunity to link regional patterns of ocean density change and water mass transformation (Zika et al., 2021) to coastal sea level change that is the result of a cross-shore mass redistribution. In the North Atlantic, Z. Li et al. (2023) identify mode and intermediate waters in particular to be a reservoir of excess atmospheric heat taken up by the ocean and discuss changes in circulation and eddy activity (e.g., Martinez-Moreno et al. (2021)). In this work, we evaluate these changes and identify a mechanistic relationship linking subtropical North Atlantic temperatures and coastal sea level south of Cape Hatteras. This relationship has been indirectly revealed in recent observations of subtropical North Atlantic heat content change and related to a decline in mode water production (Stevens et al., 2020), meridional heat convergence (Volkov et al., 2019; Zhang et al., 2024), and coastal flooding (Volkov et al., 2023). While a similar connection between coastal and offshore sea level has been evaluated with respect to interannual variability in the annual cycle and westward propagating steric anomalies (Calafat et al., 2018), the static equilibrium response to offshore steric sea level change has not, to our knowledge, been explored. The results subsequently presented here reveal details of this coastal-open-ocean connection from a new vantage point and, in this region, highlight the importance of mode water heat content.

Expectations as to how offshore changes in temperature and salinity are communicated to the coast derive from theory in which seafloor geometry is important. Along a Northern Hemisphere western boundary, in the presence of a wide continental shelf and steep continental slope, mean sea level associated with subtropical and subpolar gyres decreases shoreward and poleward (Minobe et al., 2017; Wise et al., 2018; Wise, Hughes, et al., 2020; Wise, Polton, et al., 2020). This mean structure can be expected from the conservation of potential vorticity, with coastal sea level modified by equatorward-propagating coastally trapped waves. Together, sea level change at any point along the coastline can be expressed as the combined effect of along-coast wave and across-slope transport processes.

In adopting a complementary framework that focuses on changes to this time-mean sea level structure, this analysis addresses the following question: *How do upper ocean heat content changes contribute to coastal sea level change across seasonal to interannual timescales?* While the framework developed by Wise et al. (2018) details dependence on bathymetric features, we explore offshore variability and resulting coastal changes. Using a 30-year reanalysis-forced high-resolution (1/12-degree) regional ocean simulation developed at NOAA's Geophysical Fluid Dynamics Laboratory (GFDL) (Ross et al., 2023), we find coastal sea level south of Cape Hatteras to covary with heat content change throughout the subtropical North Atlantic at monthly to interannual timescales. This heat content change is linked to mode water temperature and Gulf Stream positioning. These

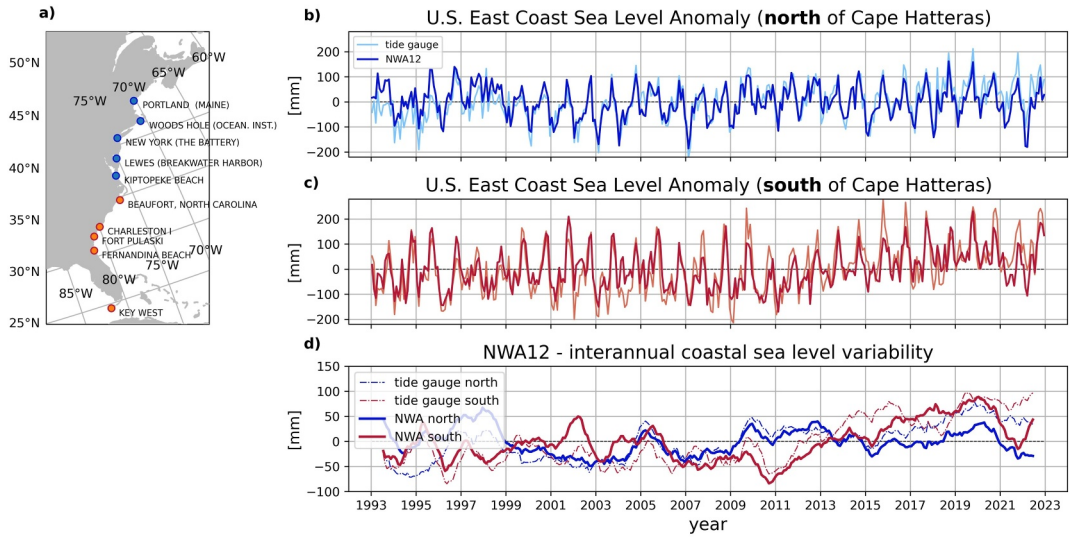

Figure 1. (a) Locations of 10 tide gauge stations used to create north and south composite sea level anomaly timeseries. (b) 1993–2023 composite sea level anomalies north of Cape Hatteras. Tide gauge measurements (light blue) are defined relative to the total time mean and adjusted to remove inverted barometer and vertical land motion contributions. Equivalent NWA12 sea level anomaly time series is in dark blue. (c) Same as (b), but for the region south of Cape Hatteras. (d) 12 month low-pass filtered tide gauge and NWA12 composite sea level anomalies.

results establish the groundwork for improving coastal sea level prediction (Dusek et al., 2022; Frederikse et al., 2022; Jevrejeva et al., 2024; Long et al., 2021) and provide a physical basis for understanding seasonal to interannual changes about which higher frequency variability drives increasingly frequent coastal flooding. The remainder of this manuscript describes the model used in this study, assesses model fidelity, details the relationship between coastal mass-driven (manometric) and offshore density-driven (steric) sea level changes, explores drivers of offshore steric variability, and quantifies the fraction of coastal sea level variance statistically accounted for by subsurface warming-driven mass redistribution. A discussion and conclusion place these results in greater context and set the stage for future work in other regions.

2. MOM6-NWA12 Regional Ocean Simulation and Sea Level Variance Decomposition

This analysis utilizes the recently developed Northwest Atlantic regional ocean model, NWA12 (Ross et al., 2023). A product of the regional Modular Ocean Model 6 (MOM6) development effort, this model comprises 75 native vertical coordinate layers with 1/12° (5–9 km) horizontal grid spacing and an expanded domain [98°W-36.08°W, 5.27°N-58.16°N] compared to past similar regional ocean models. NWA12 was selected for this analysis because during development, particular attention was given to improved representation of U.S. East Coast ocean circulation and the Gulf Stream. Furthermore, ongoing developments to increase horizontal resolution, incorporate finer scale atmosphere-ocean interactions, and integrate this model into a downscaling predictive framework motivate continued consideration of the analysis framework employed here and its application in new settings. A 30-year reanalysis-forced hindcast simulation was carried out from January 1993 to December 2022 using GLORYS12 ocean (Lellouche et al., 2021), ERA5 atmospheric (Hersbach et al., 2020), and TPXO9 tidal (Egbert & Erofeeva, 2020) boundary conditions. This model includes river discharge and astronomical tidal forcing (Alfieri et al., 2020) and uses 1 Jan 1993 GLORYS12 temperature and salinity fields as initial conditions. As a Boussinesq model, volume change occurs only as a result of volume gain or loss through the boundaries. Subsequent analyses use model monthly mean sea surface height, ζ, defined relative to the model geoid, potential temperature, θ, defined relative to the ocean surface, in situ density, ρ, potential density, defined relative to the ocean surface, ρ_θ, and ocean bottom pressure, p_b, computed according to the hydrostatic equation used by the model and ignoring atmospheric loading.

Simulated coastal sea level variability north and south of Cape Hatteras compares favorably to observations from 10 tide gauge stations (Figure 1a). Composite north and south time series are calculated as the mean of five atmospheric pressure- and vertical land motion-adjusted monthly tide gauge measurements obtained from the

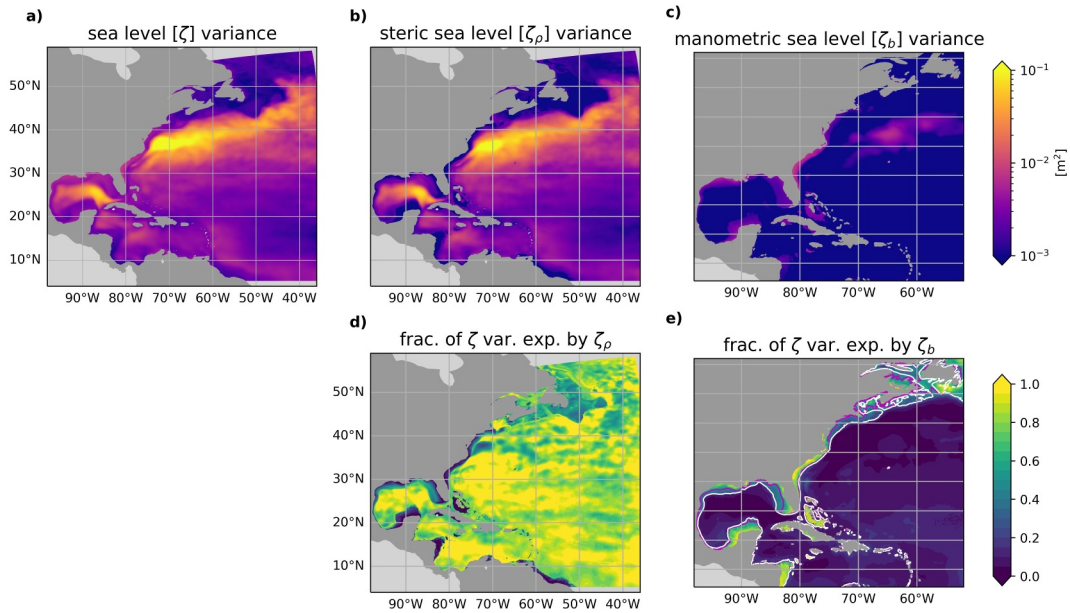

Figure 2. (a) 1993–2023 NWA12 sea level variance (note the log color scale). (b) Steric sea level, ζ_ρ, variance. (c) Manometric sea level, ζ_b, variance. (d)–(e) Fraction of ζ variance statistically accounted for by ζ_ρ and ζ_b. The white contour identifies the 150 m isobath and the purple contour that where 50% of the sea level variance is statistically accounted for by manometric sea level variance. Note changes in axis limits in panels c and (e).

Permanent Service for Mean Sea Level (Hammond et al., 2021; Hersbach et al., 2023; PSMSL, 2023) and compared to model sea level time series, adjusted to include the global steric effect (Griffies & Greatbatch, 2012) and constructed from composites averaged across the same locations (Figures 1b and 1c). Time series are referenced to have a zero mean and resulting north/south model-observation correlations both exceed 0.8 despite a weaker long-term positive sea level trend north of Cape Hatters in NWA12. This and all subsequent correlation coefficients are stated only when p-values, normally distributed probabilities of uncorrelated time series, are below 1%. Key resolved features include a seasonal cycle, with greater amplitudes at lower latitudes linked to thermal expansion/contraction, and nonstationarity in coastal sea level covariance north and south of Cape Hatteras, a variability that has been linked to the NAO (Feng et al., 2024; Woodworth et al., 2016). While interannual sea level variability north and south of Cape Hatteras is comparable between ∼2000 and ∼2008, rates of sea level rise south of Cape Hatteras increase substantially beginning in ∼2010 and remain elevated through the end of the decade (Figure 1d). South of Cape Hatteras, the time-mean cross-Gulf Stream sea level gradient is similar to observations as is the latitude of separation, a feature realized in simulations with higher horizontal resolution (Chassignet & Marshall, 2008). The latitudinal position of the Gulf Stream also tracks observations, but eastward flows are a bit weaker and more variable (Ross et al., 2023).

Following Yin et al. (2010) and Griffies and Greatbatch (2012), we seek to decompose sea level changes into mass and density changes. For a hydrostatic ocean, the time tendency of sea level at a given latitude and longitude can be decomposed into contributions from local ocean mass (manometric) and density (steric) change (Figures 2a–2c) as

$$\frac{\partial \zeta}{\partial t} = \frac{1}{\rho_0 g}\frac{\partial (p_b - p_a)}{\partial t} - \frac{1}{\rho_0}\int_{-H}^{\zeta}\frac{\partial \rho}{\partial t}\,\mathrm{d}z. \tag{1}$$

In this simulation, atmospheric pressure is not felt by the ocean $(p_a = 0)$, so bottom pressure p_b/g is equivalent to ocean mass per horizontal area of the fluid column; $g = 9.81$ m s^{-2} is gravitational acceleration, H is seafloor depth, ρ is in situ density, and $\rho_0 = 1035$ kg m^{-3} is a reference density. This relationship is derived by vertically integrating and then differentiating in time the hydrostatic balance and making the Boussinesq approximation. In the limit of ocean depth going to zero, nearly all sea level change can be understood as local mass change

(Figures 2d and 2e, purple contour). The depth dependence of this relationship reveals a majority of near-coast sea level change to reflect local mass change (e.g., Vinogradova et al. (2007)) that can be interpreted in the Wise et al. (2018) Northern Hemisphere western boundary framework as driven by either equatorward-propagating coastally trapped anomalies or cross-shore mass redistribution (This framework omits consideration of local forcing factors like longshore wind). These changes in mass occur rapidly in response to forcing while offshore changes in ζ overwhelmingly reflect changes in ζ_ρ and adjust at longer baroclinic timescales (Forget & Ponte, 2015; McWilliams et al., 2024). Subsequent analyses express ocean bottom pressure changes, Δp_b, in terms of manometric sea level change,

$$\Delta\zeta_b = \Delta p_b/(\rho_0\, g), \tag{2}$$

and use model in situ density to calculate steric sea level change,

$$\Delta\zeta_\rho = -\frac{1}{\rho_0}\int_{-H}^{\zeta} \Delta\rho \; \mathrm{d}z. \tag{3}$$

Potential temperature, θ, and potential density, ρ_θ, referenced to the ocean surface are used to quantify mode water layers and temperature change.

3. Analysis and Results

3.1. Mass and Density-Driven Sea Level Change

Initial consideration of the relationships among ζ_ρ, ζ_b, and H at lower frequencies reveals a distinct pattern of coastal and open-ocean covariability that largely matches observations (Figure 3). Linear ζ_b' trends, defined for this field only as anomalies to the domain average trend and fit over two 6-year periods, reveal low-frequency changes in shelf loading that vary in concert with offshore ζ_ρ change (Figures 3e–3h). All other prime use denotes anomalies to a time mean. These 6-year periods were selected to highlight distinct patterns of observed variability and, importantly, a change in interannual variability beginning in 2010 and previously reported by Dangendorf et al. (2021); Yin (2023); Z. Li et al. (2023); and Volkov et al. (2023). Comparison between altimeter measurements and NWA12 fields is made as an initial interrogation of the model to consider the extent to which large scale patterns of variability and change are resolved. While altimeter measurement errors increase approaching the coast due to instrumental biases (Vignudelli et al., 2019), modeled and observed trend patterns both suggest distinct variability on the continental shelf and offshore. These and all subsequent trend estimates are considered significant where they exceed a standard error defined as one standard deviation of 100 Fourier phase-scrambled trend estimates (Steinberg et al., 2024).

Over the 2002–2007 period (Figures 3c– 3e and 3g), mass was lost over the shelves as offshore ζ_ρ decreased. These mass changes are defined relative to domain average mass gain/loss (Figure 3i) such that they can subsequently be termed a redistribution. During the 2012–2017 period (Figures 3d– 3f and 3h), mass was gained on the shelf, south of Cape Hatteras and in the Gulf of Mexico, while offshore, ζ_ρ rose throughout the subtropical North Atlantic and particularly south of the Gulf Stream extension. These onshore and offshore trends are consistent with the redistribution model described by Landerer et al. (2007). Relative manometric and steric trend contributions to the total sea level trend again show that mass changes are more significant in shallow regions, even as waters on the shelf warm (Figures 3d–3f). Domain average sea level, volume, and mass variability (Figure 3i) place these compensating density and mass redistribution trends in a greater context and show that they occur in addition to 'global' manometric and thermosteric sea level rise (i.e., positive trends in domain average volume and sea level with the global steric correction (Griffies & Greatbatch, 2012)).

The patterns of these ζ_b' and ζ_ρ trends suggest that ζ_b' trends may partly reflect a static response to ζ_ρ changes. This framework was first developed by Landerer et al. (2007) linking open-ocean and coastal changes that are broadly framed as a static equilibrium response equivalent to inverted barometer adjustment (Greatbatch, 1994; Steinberg et al., 2024). In this case, static equilibrium refers to one component of the full equilibrium response that includes a dynamical adjustment. Using the NWA12 discrete layered framework, anticipated manometric sea level change $\zeta_{b_i}^*(t)$ can be determined as a static response to density change as

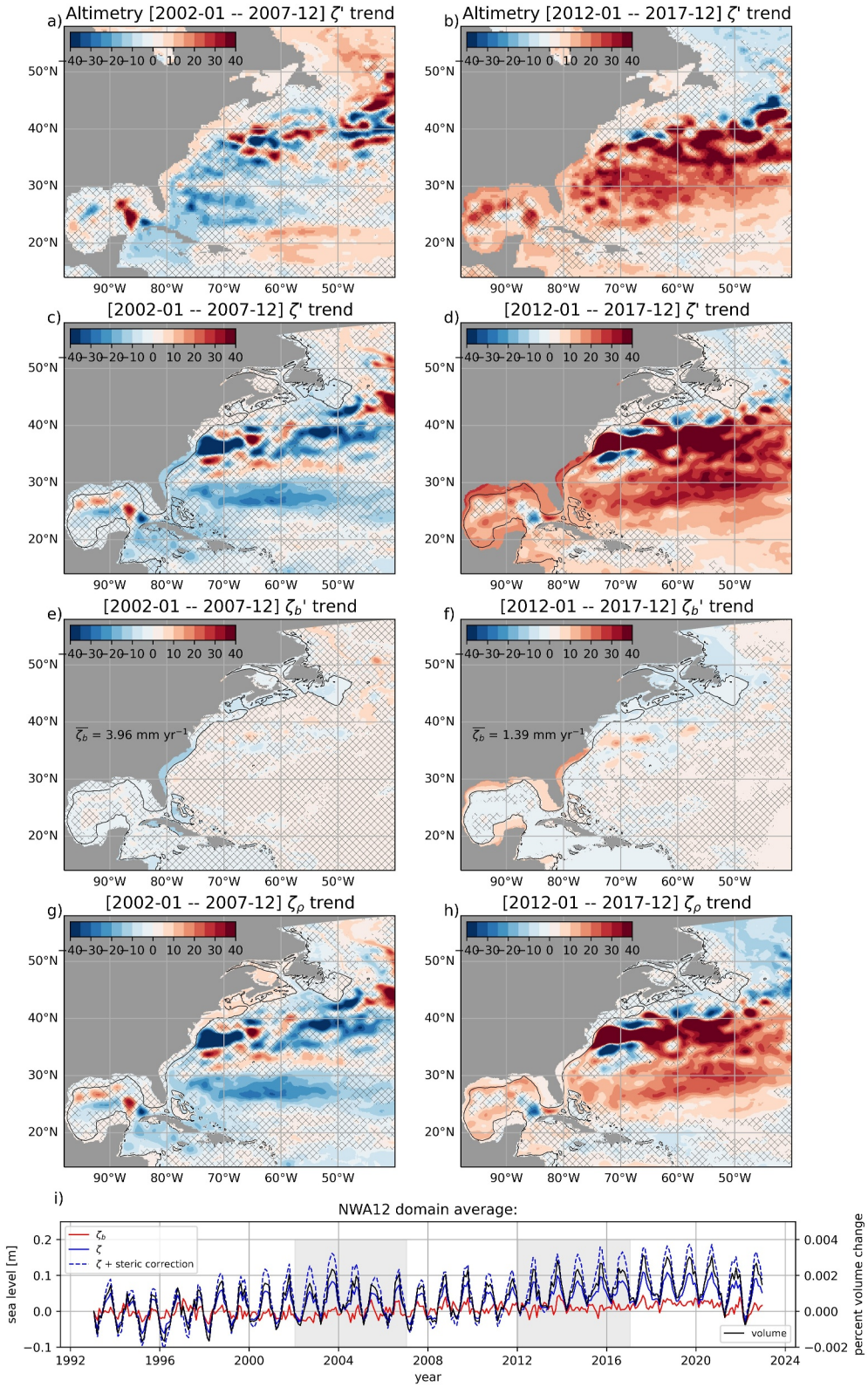
a) Altimetry [2002-01 -- 2007-12] ζ' trend
b) Altimetry [2012-01 -- 2017-12] ζ' trend
c) [2002-01 -- 2007-12] ζ' trend
d) [2012-01 -- 2017-12] ζ' trend
e) [2002-01 -- 2007-12] ζ_b' trend
f) [2012-01 -- 2017-12] ζ_b' trend
g) [2002-01 -- 2007-12] ζ_ρ trend
h) [2012-01 -- 2017-12] ζ_ρ trend
−40 −30 −20 −10 0 10 20 30 40
50°N
40°N
30°N
20°N
90°W 80°W 70°W 60°W 50°W
ζ_b = 3.96 mm yr^−1
ζ_b = 1.39 mm yr^−1
i)
NWA12 domain average:
ζ_b
ζ
ζ + steric correction
volume
sea level [m]
percent volume change
year
1992 1996 2000 2004 2008 2012 2016 2020 2024

Figure 3.

$$\zeta^*_{b_i}(t) = \frac{1}{\rho_0}\sum_{k=1}^{i}\left(1-\frac{A_k}{A_s}\right)\left(\rho_k(t)-\overline{\rho_k}\right)h_k - \frac{1}{\rho_0}\sum_{k=i+1}^{N}\frac{A_k}{A_s}\left(\rho_k(t)-\overline{\rho_k}\right)h_k. \quad (4)$$

Here, $\zeta^*_{b_i}$ changes in time, t, and within each layer, i, are a function of the distribution of layer areas with depth, layer mean density anomalies relative to a time mean, $\left(\rho_i - \overline{\rho_i}\right)$, and layer thickness, h_i. Estimated ζ^*_b changes within each layer reflect the combined effect of density changes across all layers. Surface area, A_s, and subsurface layer areas, A_i, need to be determined considering geographical and physical factors such that horizontal density variability within these areas is minimal (i.e., density anomalies in Equation 4 represent a horizontal average within layers). The spatial patterns of these surface and subsurface density anomalies may reflect patterns of ocean circulation, the effects of eddies and horizontal mixing, or surface buoyancy forcing. In the North Atlantic, subpolar and subtropical gyres shape upper ocean temperature and salinity distributions and provide an initial physical basis upon which to consider warming-driven mass redistribution. While Greatbatch (1994) and Landerer et al. (2007) develop and apply their models globally, we seek to apply it regionally (Bingham & Hughes, 2012). With a region of influence loosely identified, offshore density changes are next explored in more detail, and the expected coastal sea level response is calculated and compared to coastal ζ'_b. This approach is adopted to reveal the contribution of this adjustment process relative to all other local and remote forcings.

3.2. Subtropical Mode Waters

As explained in the preceding section, we are exploring the hypothesis that coastal sea level changes in the region arise partly from heat and density changes over the adjacent open ocean. Motivated by recent results that emphasize mode waters as a reservoir of excess heat taken up from the atmosphere (Z. Li et al., 2023) and establish a link between subtropical North Atlantic heat content and coastal sea level (Volkov et al., 2019, 2023), we consider NWA12 subtropical mode water (STMW) change as a first step in defining an offshore region affecting coastal sea level (Figure 4). Traditionally, the term North Atlantic subtropical mode water, or 18°C water, has been used to reference a lens of weakly stratified, low potential vorticity waters below the seasonal mixed layer and roughly 250 m thick (Kwon & Riser, 2004). Waters between bounding isopycnals are seasonally ventilated along and northward of the Gulf Stream extension connecting water mass volume and heat content to annual and interannual variability associated with the NAO (Figure 5). Bounding shallow and deep potential density surfaces are here defined as $\rho_\theta = 1025.2$ kg m^{-3} and $\rho_\theta = 1026.5$ kg m^{-3} to include shallower layers as well as multiple previously employed stricter mode water definitions (Gan et al., 2023; Kwon & Riser, 2004) such that upper ocean density change may be broadly considered and related to the Gulf Stream. These isopycnals define a lens on average greater than 200-m thick spanning ocean depths of 50–500 m (Figures 4a–4c).

The thickness of this lens varies seasonally as the upper layers are ventilated during wintertime mixing and at interannual timescales as the latitude of the Gulf Stream extension shifts north or south (Figures 4d and 4e). An areal mask is subsequently defined for evaluating the static equilibrium model introduced in the preceding section and relating open ocean and coastal conditions using the mean 200-m thickness criteria extending west to the coast (Figure 4f). The near-coast extent of this mask is initially defined as a zonal westward extension of the 200-m thickness criteria as in Figure 4e. While the expectation is that coastal sea level in the Gulf of Mexico and Caribbean should also be affected by changes in the subtropical gyre (i.e., Wise et al. (2018) show a damped, equatorward shift of the gyre sea level anomaly), this choice was made to initially emphasize a more local response.

In focusing on and adopting this definition of subtropical mode waters, upper ocean density changes can be evaluated in a regional climate scale context. Interannual variability in atmospheric forcing, meridional heat transport, and Gulf Stream extension position are integrated into a record of upper ocean heat content change that affects coastal sea level. Throughout this 30-year model simulation, the Gulf Stream extension position is

Figure 3. (a) Satellite altimeter derived 2002–2007 sea level anomaly trend [mm yr^{-1}]. Hatched area denotes the region where calculated trends do not exceed standard error. (b) Same as (a), but for the 2012–2017 period. NWA12: (c) 2002–2007 linear sea level anomaly trend. Black contour identifies the 150 m isobath. (d) Same as (c), but for the 2012–2017 period. (e)–(f) Manometric sea level ζ'_b trends over the same 6-year periods and defined relative to the model domain average trend ($\zeta'_b = \zeta_b - \langle\zeta_b\rangle$). (g)–(h) Steric sea level ζ_ρ trend over the same 6-year periods. (i) Domain average sea level (blue), steric-corrected sea level (dashed blue), manometric sea level (red), and model volume (black) defined relative to the first timestep. Shaded regions denote the periods over which above trends are fit.

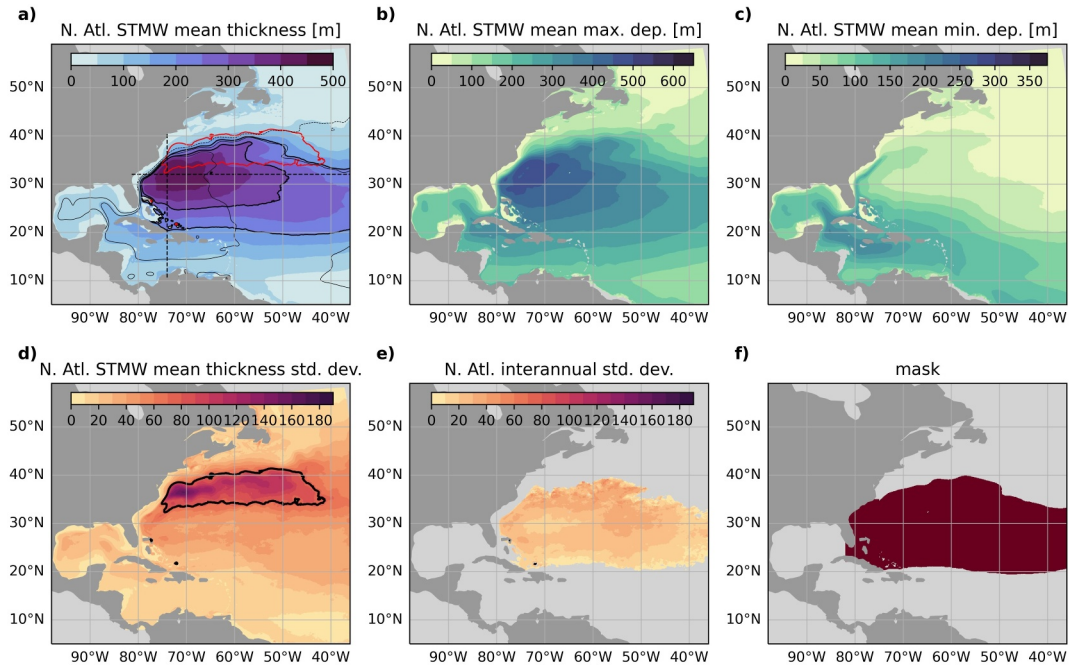

Figure 4. (a) Time-mean STMW thickness: 200 and 300 m contours in black, $\zeta' = -0.25$, 0, and 0.25 m in gray, and STMW thickness standard deviation = 75 m in red. Black dashed lines are the locations of meridional and zonal cross sections in Figure 7. (b) Time-mean depth of $\rho_\theta = 1026.5$ kg m^{-3}. (c) Time-mean depth of $\rho_\theta = 1025.2$ kg m^{-3}. (d) Standard deviation of STMW thickness [m]. Black contour identifies the 75-m value. (e) 12 month low-pass filtered standard deviation of STMW thickness. A mask is applied to show regions where the time-mean thickness exceeds 200 m. (f) 200-m time-mean STMW thickness mask extended west to include coastal regions south of Cape Hatteras.

comparable to observations (Figure 6a, Ross et al. (2023)) with the index used to make this comparison (Perez-Hernandez & Joyce, 2014; Ross et al., 2023) tracking zonal mean north/south displacement of the Gulf Stream extension from sea surface height measurements and variance. We find both STMW area and volume-mean potential temperature anomalies, defined as

$$\overline{\theta'} = \frac{1}{V}\iiint_{z(\rho_\theta=10265.5)}^{z(\rho_\theta=1025.2)} \theta'\, dx'\, dy'\, dz' \tag{5}$$

to track with this position (Figures 6a–6c, Gulf Stream/$\overline{\theta'}$ correlation of 0.69). Mode water area and volume, V, are calculated at each monthly increment and summed across longitudes and latitudes where the vertical distance

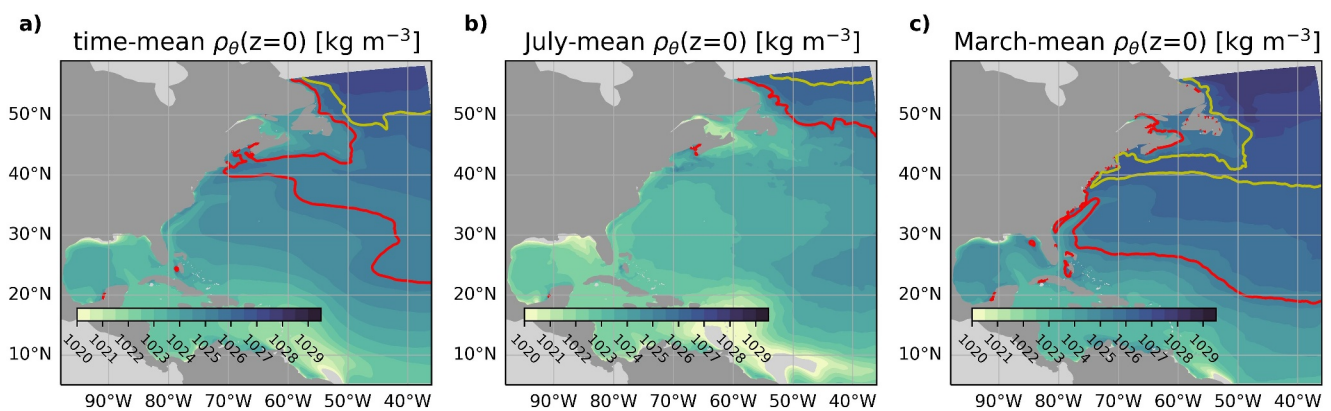

Figure 5. (a) NWA12 time-mean surface ρ_θ ($\rho_\theta = 1{,}025.2$ and $\rho_\theta = 1{,}026.5$ kg m^{-3} are in red and yellow, respectively). (b) July mean surface ρ_θ. (c) March mean surface ρ_θ.

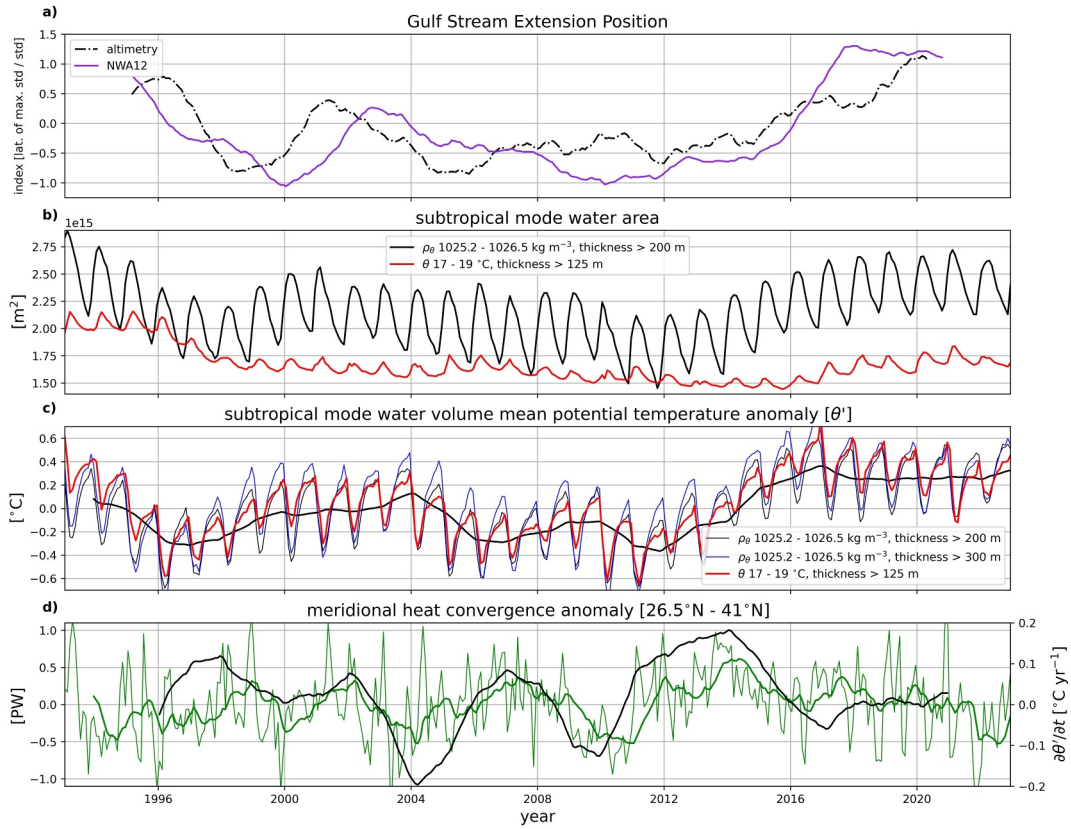

Figure 6. (a) NWA12 Gulf Stream index (purple) defined as the longitudinal mean of ζ at latitudes of maximum ζ standard deviation (normalized by standard deviation) (Ross et al., 2023). Observation-based estimate is in black. (b) STMW area with thickness greater than 200 m. Thickness between 17 − 19°C isotherms is in red. (c) STMW volume-mean θ' (black), representing an average within bounding isopycnals and where thickness is greater than 200 m. The heavy black line is a 24 month low-pass filtered equivalent. The blue line shows that for a 300 m-thickness criteria and red for that between 17°C and 19°C isotherms. (d) Monthly (light green) and 12 month low-pass filtered (dark green) meridional heat convergence in petawatts between 26.5°N and 41°N (Volkov et al., 2023). The time rate of change, calculated as a rolling 5-year linear fit to volume-mean potential temperature anomalies in (c), is in black.

between bounding isopycnals is equal to or greater than 200 m. Reference comparison is made using traditionally defined 17 − 19°C isotherms as vertical limits of integration (Figures 6b and 6c red time series), revealing similar patterns of volume-mean temperature change within a region of smaller area and less interannual variability. In general, larger values of the Gulf Stream index, indicating a northward deflection, correspond to both larger mode water area and warmer volume-mean potential temperature. Since approximately 2012, the Gulf Stream extension has remained in this state through the end of the simulation as subtropical waters warmed rapidly.

Meridional heat transport convergence between 26.5°N and 41°N, especially during the warming period between ≈2012 and ≈2017, similarly shows this rate of change of subtropical North Atlantic heat content (Figure 6d). These results are similar to those derived from recent observations (Volkov et al., 2023; Zhang et al., 2024) highlighting in-phase variability with NAO, but here, we consider upper ocean heat content change as possibly additionally influenced by remote forcing outside of this latitude band. The vertical extent of seasonally ventilated isopycnals and the spatial patterns of interannual subsurface density variability thus far considered (Figures 3c and 3d) suggest a majority of subtropical North Atlantic heat content change to reflect mode water change (Figure 7). Depth-latitude and depth-longitude density trends during the 2012–2017 period of elevated sea level rise highlight both a Gulf Stream shift and warming throughout the lens of mode waters defined in Figure 4 (Figures 7d and 7e). Averaging across latitudes and longitudes within the 200-m mode water thickness mask (Figure 4e) reveals the depth dependence of the frequency of density and temperature change (Figures 8a and 8b). An apparent seasonal cycle in this region regularly penetrates to ∼150 m while lower frequency changes are

largely surface-intensified, penetrate to deeper depths over the course of many months, and are primarily confined to the upper 500 m. These changes are consistent with Argo float-observed temperature anomalies, measured since 2004 (Figure 8c). As with model output, these anomalies highlight the depth extent of the significant warming event beginning around 2014 that is coincident with a northward shift of the Gulf Stream extension and an increase in STMW area (Figure 6).

To summarize, this characterization and evaluation of upper ocean density change in the subtropical North Atlantic was motivated by consideration of the pattern of offshore steric and onshore manometric sea level trends (Figure 3). Over the 2012–2017 period, sea level rose rapidly on the shelf, but only south of Cape Hatteras. This occurred concurrently with upper ocean STMW warming, and thus motivates and guides the application of the mass redistribution framework introduced in Section 2.

3.3. Mass Redistribution and Coastal Sea Level

Having determined seasonal to interannual ζ_ρ variability throughout the subtropical North Atlantic to largely reflect warming and cooling of waters in the upper ~750 m (Figures 7 and 8), we next estimate a ζ_b' response expected from Equation 4. This expected static equilibrium response is understood as a cross-shore mass redistribution driven by offshore density change below the continental shelf break. As discussed by Landerer et al. (2007) and Steinberg et al. (2024), the static response of interest follows a rapid barotropic adjustment to some initial perturbation in a similar manner to the inverted barometer effect (Greatbatch, 1994). In this case, we apply a similar framework to a distinct region rather than globally and define a regional mask as one shaped by water mass characteristics. Importantly, this shoreward mass redistribution occurs only when density changes are sufficiently deep (i.e., where the fractional ocean area of some subsurface layer A_i is less than the total surface area A_s throughout the region of interest).

Predicted ζ_b^* change at $z = -5$ m, corresponding to the shallowest model seafloor depths (Figure 9a; orange time series), compares favorably to model ζ_b' averaged across depths shallower than 100 m and within the STMW masked region in Figure 4e (Figure 9a; blue time series). In this redistribution framework, shelf mass gain and loss occur at seasonal timescales and are at least partly the result of the seasonal maximum mixed layer depth extending below the shelf break (Figure 9c). This framework for understanding coastal sea level change also has explanatory power at interannual timescales and appears linked to STMW heat content change and Gulf Stream position variability (Figure 9b). To emphasize the requirement of offshore subsurface density change to realize cross-shore mass redistribution, Equation 4 was evaluated over only the model's shallowest six layers ($0 > z > -27.5$ m) (Figure 9a; black time series). This calculation highlights that density change throughout these shallow layers drives a significantly weaker mass redistribution with no interannual variability. While density changes in these layers are not small, mass redistribution is minimal because the subsurface layer areas are nearly as large as the region of interest's total surface area.

At seasonal and interannual timescales, there appears a robust relationship between ζ_b' and $\zeta_b^*(z = -5$ m) (Figure 10). Expected mass loading near the coast is regressed onto ζ_b' at all locations in the model where ocean depths are less than 1,000 m (i.e., depths where a dominant fraction of ζ variance is statistically accounted for by ζ_b) and shown at the 95% confidence level evaluated from a Student's *t*-test (Figures 10a and 10b). A positive relationship appears all along the coast south of Cape Cod, increasing equatorward and in shallow regions of the Caribbean. When low-pass filtered to remove the seasonal cycle, the extent of this positive relationship is limited to regions south of Cape Hatteras. This suggests that seasonal mass loading on the shelf occurs over broad regions as a result of seasonal mixing penetrating to depths deeper than the shelf break. Lower frequency variability on the shelf, however, is linked to offshore density changes in the subtropical North Atlantic only south of Cape Hatteras. This difference suggests interannual sea level variability south of Cape Hatteras is linked to subtropical North Atlantic subsurface density change that is absent north of Cape Hatteras. The influence of the subtropical gyre and expectation of equatorward-propagating coastally trapped waves thus explains periods of decreased East Coast sea level covariance as the result of increased density variability south of the Gulf Stream extension. In reconsidering the 6-year trends shown in Figure 3, ζ_b^* trends are fit over the same periods and mapped onto depths corresponding to each model layer depth (Figure 11). Similar spatial patterns across both periods suggest low-frequency shelf loading to be driven by this mass redistribution mechanism.

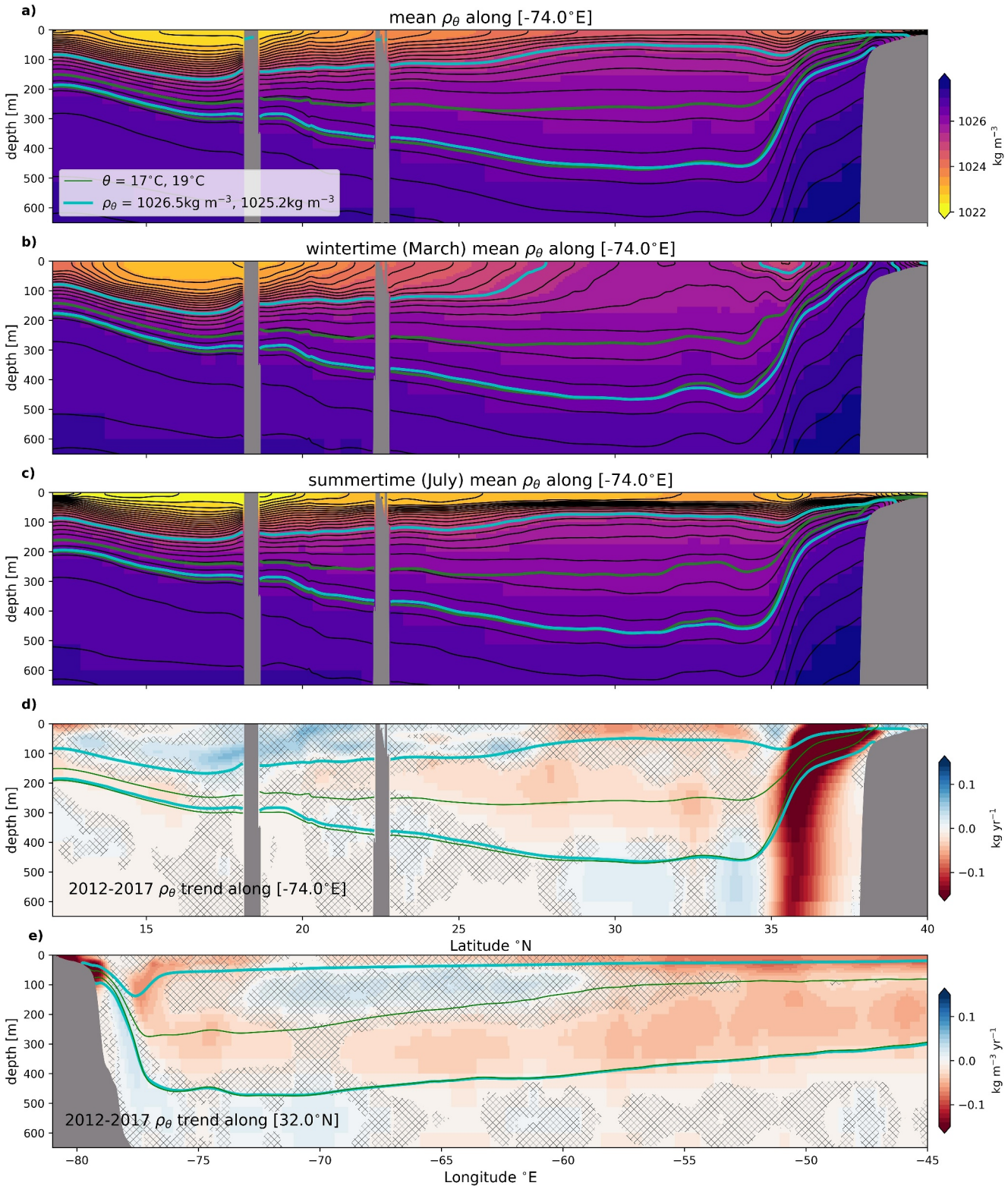

Figure 7. (a) NWA12 time-mean depth-latitude ρ_θ cross section at 74°W. Blue contours are the 1,025.2 and 1,026.5 kg m^{-3} isopycnals, and green contours are the 17 and 19° isotherms. (b) Same as (a) for 30-year March mean. (c) Same as (a) for 30-year July mean. (d) 2012–2017 linear ρ_θ trend. (e) 2012–2017 linear ρ_θ trend along the 32°N longitudinal transect (dashed lines in Figure 4). In (d) and (e), hatched areas correspond to regions where trends do not exceed standard error.

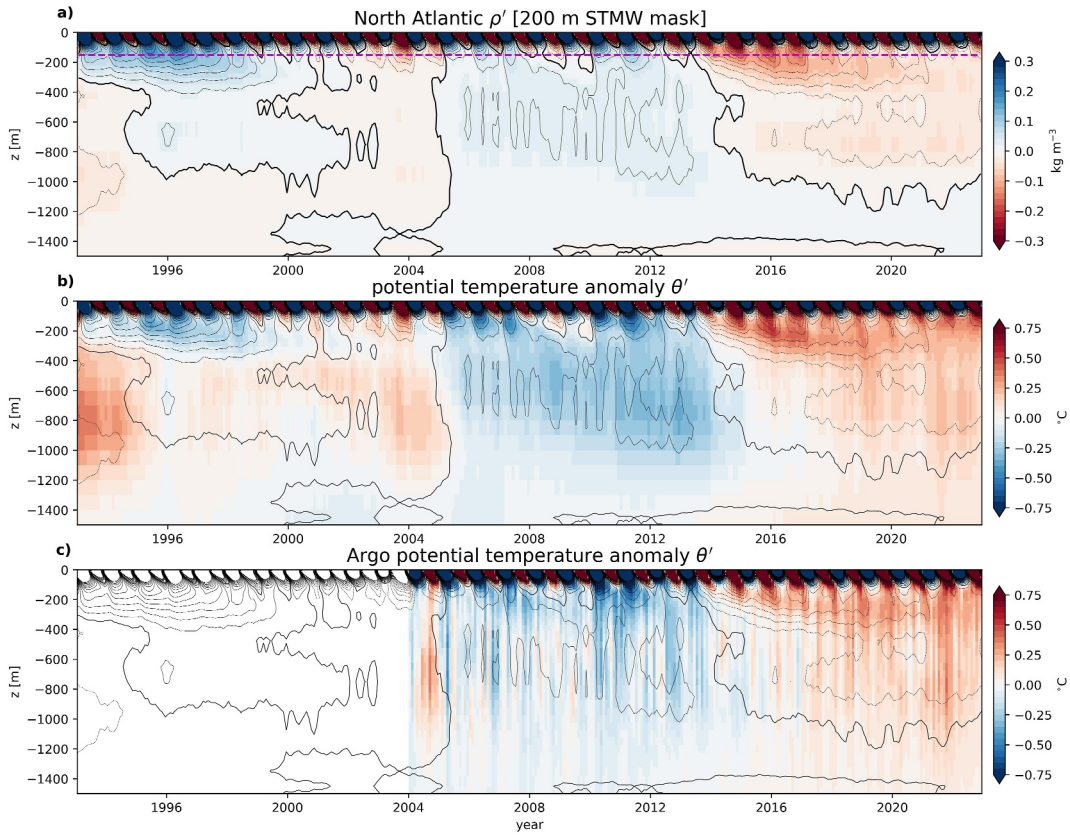

Figure 8. (a) Hovmoller diagram of ρ_θ', defined relative to a 30-year time-mean profile and averaged across the masked region in Figure 4e. The horizontal dashed line in purple is $z = -150$ m (b). Same as (a) but for θ'. Contoured lines are ρ_θ' levels in (a). (c) Argo floats-derived equivalent to (b) (Roemmich & Gilson, 2009). Observations begin in 2004, and contoured lines are ρ_θ' levels in (a).

A region of similar shape, but lesser extent appears in calculating the fraction of ζ_b' variance statistically accounted for by $\zeta_b^*(z = -5\text{ m})$ (Figures 10c and 10d). The largest values, greater than 0.5, are found across the broad shallow shelf surrounding the Bahamas, likely a result of proximity to subtropical heat content change and its location east of the Florida Current. When low-pass filtered to remove a seasonal cycle and incidentally other subannual coastal variability (Figure 10d), the fraction of variance accounted for increases to ∼0.5 over a broader region of the shelf south of Cape Hatteras and into the Gulf of Mexico.

The expected near-coast $\zeta_b^*(z = -5\text{ m})$ change covaries with ζ' more broadly (Figures 10e and 10f). The fraction of ζ variance statistically accounted for by $\zeta_b^*(z = -5\text{ m})$ exceeds 0.5 along the continental shelf and slope, including in regions north of Cape Hatteras. As in Figure 10b, this relationship along the shelf is subsequently restricted to regions south of Cape Hatteras after applying the same low-pass filter to remove a seasonal cycle, suggesting that a component of the shelf ζ seasonal cycle is the result of cross-slope mass redistribution that occurs when seasonal mixing penetrates below the shelf break. The largest values of interannual ζ variance statistically accounted for by $\zeta_b^*(z = -5\text{ m})$ are found on the continental shelf south of Cape Hatteras and east of the Bahamas. This pattern implies covariability between offshore ζ_ρ, the dominant driver of offshore ζ variance, and coastal ζ_b' south of Cape Hatteras, a relationship discussed by Volkov et al. (2019, 2023) as linked to meridional heat transport and NAO phasing. Connectivity between the subtropical North Atlantic and the Gulf of Mexico coastlines suggests the Gulf of Mexico feels regional heat content change that is communicated via the Loop Current (Thirion et al., 2024). These results now suggest a mechanistic understanding as to how offshore changes in heat content drive a significant fraction of coastal sea level variability.

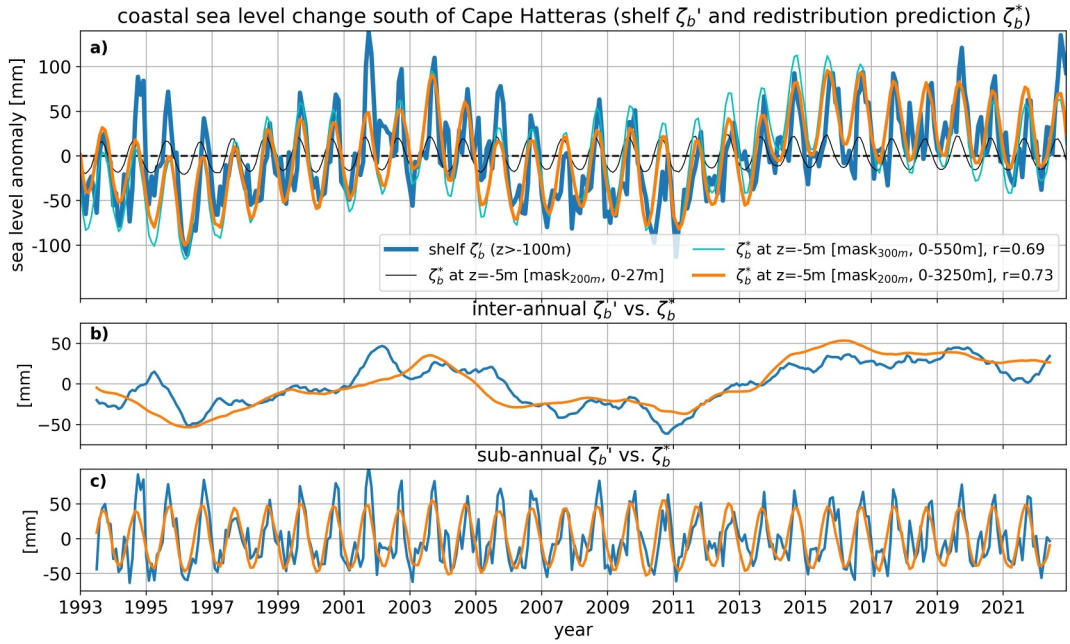

Figure 9. (a) ζ_b' (blue) versus $\zeta_b^*(z=-5\text{ m})$ (orange) where ζ_b' is averaged south of Cape Hatteras across ocean depths less than 100 m. $\zeta_b^*(z=-5\text{ m})$ corresponding to a 300-m STMW thickness mask is in cyan, and that evaluated only over the model's upper six layers (0> z > − 27m) is in black. Pearson correlation coefficients are added in the legend. (b) 12 month low-pass filtered and (c) 12 month high-pass filtered ζ_b' and $\zeta_b^*(z=-5\text{ m})$.

4. Discussions and Conclusion

Utilizing a newly developed high-resolution regional ocean simulation (NOAA GFDL's NWA12, Ross et al. (2023)), this analysis demonstrates that a relatively simple mass redistribution model can statistically explain a significant fraction of seasonal to interannual coastal sea level variance south of Cape Hatteras, in the Gulf of Mexico, and along northern Caribbean shelves. With a horizontal grid spacing of $1/12°$, this regional model faithfully reproduces 1993–2023 coastal sea level change along the U.S. East Coast (Figure 1), resolves the Gulf Stream as it separates from the slope near Cape Hatteras (Figure 6a), realizes a down coast gradient of mean sea level that coarser resolution models lack (Higginson et al., 2015), and captures recently observed upper ocean warming throughout the subtropical North Atlantic (Figures 8c and eg. Volkov et al. (2019)). Evaluation of upper ocean density change within the subtropical North Atlantic reveals mode waters, a seasonally ventilated weakly stratified water mass found just below the summertime pycnocline, to have experienced significant warming since the early 2010's (Stevens et al., 2020). At monthly and longer timescales, subsurface volume-mean temperature, a metric for this warming, covaries with the coastal sea level south of Cape Hatteras. The relationship between these two fields is interpreted as a result of shelf mass gain or loss in response to offshore warming or cooling (Figures 9 and 10, Equation 4). These offshore changes in upper ocean heat content vary with the latitudinal position of the Gulf Stream extension, a behavior that has been linked to phasing and strength of the North Atlantic Oscillation (Chi et al., 2023; Zhang et al., 2024) and meridional heat transport (Volkov et al., 2019, 2023). The mechanistic connection between open-ocean heat content change and coastal sea level identified here provides new interpretation as to the impacts of regional-scale offshore ocean warming.

In investigating the drivers of U.S East Coast sea level variability, many past studies have sought to explicitly evaluate the influence of the Gulf Stream, the role of the AMOC, and upper ocean temperatures (Chi et al., 2023; Dong et al., 2019; Ezer, 2019; Ezer et al., 2013; Little et al., 2019; Widlansky et al., 2020). As discussed by Chi et al. (2023), one difficulty in doing so arises as a result of higher frequency spatially varying patterns of recirculation that impact Gulf Stream transport and position estimates. These estimates are relevant, however, as the cross-shore sea level gradient linked to transport affects shelf sea level and modulates the effects of southward propagating coastal trapped waves (Hughes et al., 2019). In addition to these processes, we now expect a static equilibrium response to offshore density change, identified here as subsurface warming/cooling driven mass

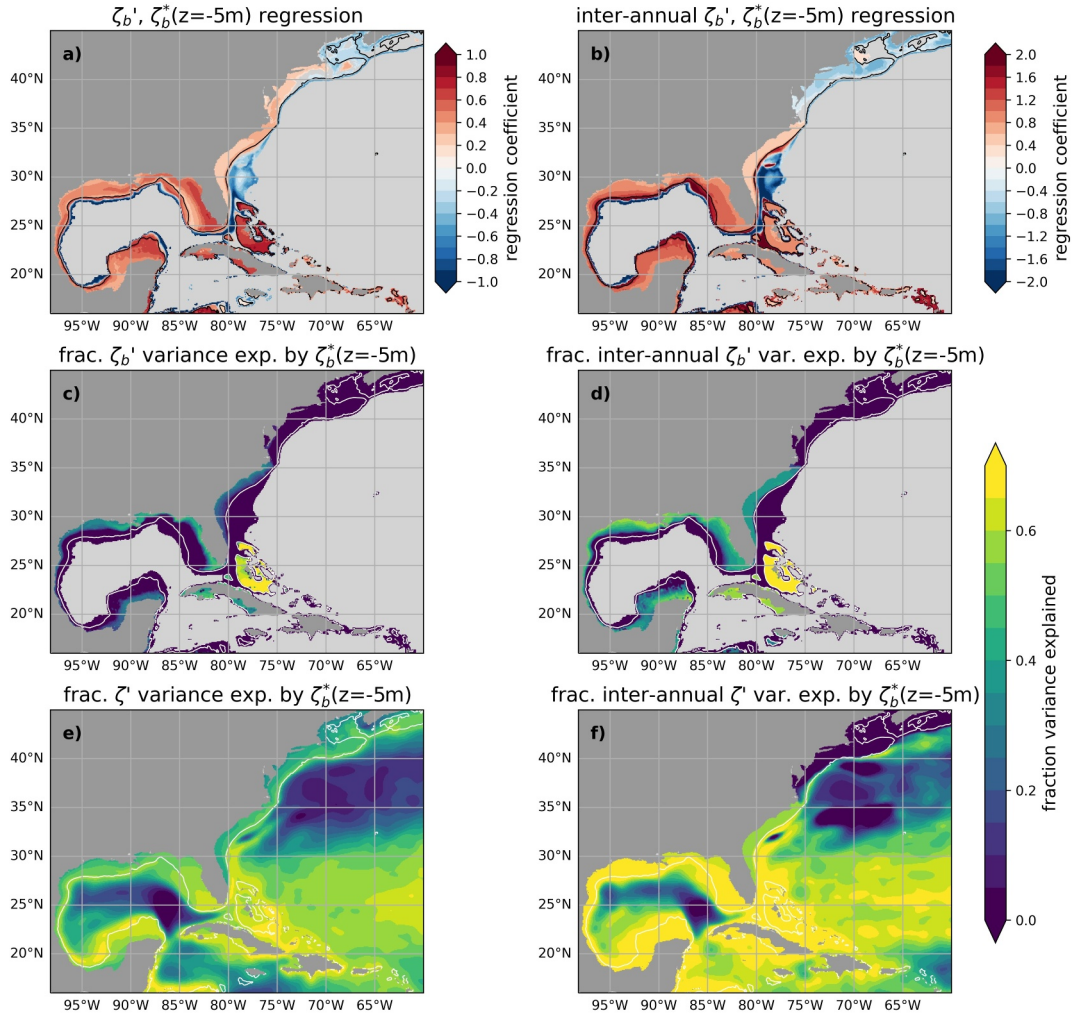

Figure 10. (a) Linear regression coefficient of $\zeta_b^*(z = -5\text{ m})$ regressed onto ζ_b'. Regression is carried out where H < 1,000 m. Colored regions show where the 95% confidence interval criteria is met. (b) Same as (a), but for interannual $\zeta_b^*(z = -5\text{ m})$ and ζ_b' (c) Fraction of ζ_b' variance statistically accounted for by $\zeta_b^*(z = -5\text{ m})$ where H < 1,000 m (b) Fraction of interannual ζ_b' variance statistically accounted for by interannual $\zeta_b^*(z = -5\text{ m})$. (e)–(f) Same as (c)–(d) but for total sea level ζ' at all grid points in the model domain.

redistribution. While this adjustment represents only one process impacting the coast, it explains approximately half of coastal sea level variance. We acknowledge that a response to offshore steric sea level change should also include a more difficult to diagnose dynamical response (e.g., cross-slope current adjustment) comprising some fraction of unexplained sea level variance near the coast (Figure 10). These results further highlight the importance of accurately simulating the Gulf Stream, the latitude of its separation from the coast, and shelf-slope bathymetry. While doing so depends on model resolution and mixing schemes (Chassignet & Marshall, 2008), poor representation of the Gulf Stream may limit many model applications to U.S. East Coast sea level prediction (Feng et al., 2024).

In addressing how open-ocean density changes are felt at the coast, Bingham and Hughes (2012) highlight the role of bathymetry in moderating offshore steric change. With density information alone, assuming no geostrophic flow at the seafloor, they explore the extent to which coastal sea level can be expressed as a cross-shelf/slope integral in bottom density along the seafloor (Bingham and Hughes (2012), Eq. 7). This approach well describes coastal sea level along eastern boundaries, but cross-shore communication along western boundary shelf and slope regions (Figure 7e) is made more complex by the presence of slope and shelf currents. Helland-Hansen (1934), Reid and Mantyla (1976), and Csanady (1979) all discuss the utility of bottom density measurements

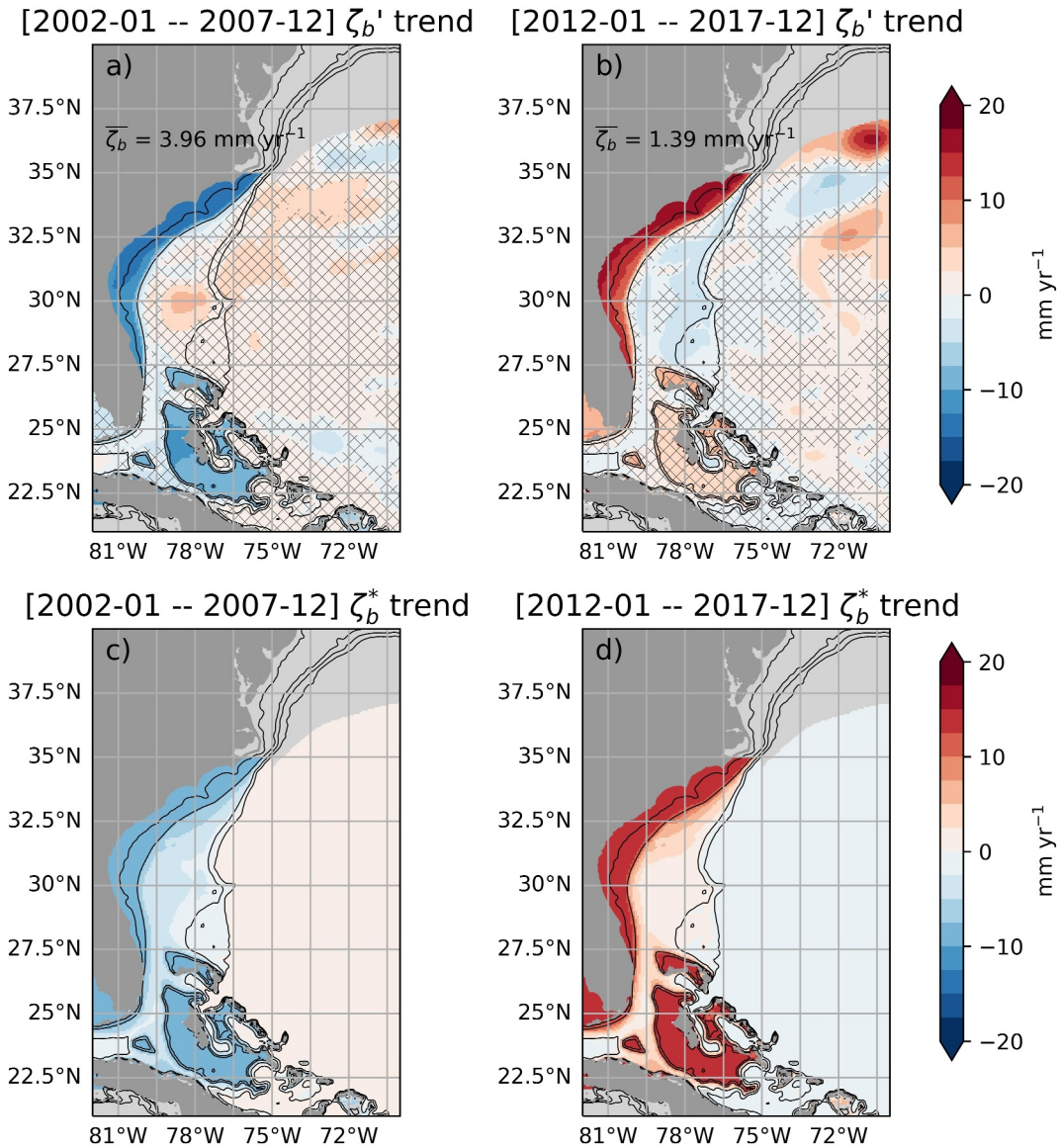

Figure 11. (a) 2002–2007 NWA12 manometric sea level trends as in Figure 3 shown for the masked region in Figure 4. Hatched area denotes the region where trends do not exceed standard error. (b) Same as (a), but for the 2012–2017 period. (c) 2002–2007 ζ_b^* trends mapped onto the model bathymetry. (d) Same as (c), but for the 2012–2017 period.

and consider this sea level adjustment near the coast. This methodology was tested in NWA12 along a zonal section east of the Georgia coastline with shelf and slope bottom density anomalies (Figure 7e) found to reproduce coastal sea level variability very well (Pearson correlation coefficient of approximately 0.9) only when integrated along the seafloor from depths greater than those where bounding STMW isopycals touch the slope. Consideration of both cross-shelf mass redistribution and shelf/slope bottom density change motivates continued work in an effort to develop a more complete expectation of a cross-slope adjustment.

Using an adjoint approach, Wang et al. (2022, 2024) reveal the added influence of subtropical and subpolar North Atlantic wind stress in driving coastal sea level change north and south of Cape Hatteras. While sea level in Nantucket, MA, is found to be primarily influenced by subpolar winds, sea level in Charleston, SC, is linked to offshore wind stress over the Gulf Stream extension. Interpreted alongside results from Volkov et al. (2019) and Zhang et al. (2024), Charleston's connectivity to the subtropical North Atlantic is realized as a link to the wind-driven circulation, ocean heat content, and AMOC-related buoyancy variations. While diagnosing the relative contributions of buoyancy and wind stress forcing on ocean heat content change are beyond the scope of this

study, our results present a mechanistic understanding of the open ocean to coast connection. One new interpretation from this study is that the mechanistic response to offshore steric sea level change may contribute to the break in U.S. East Coast sea level covariability during periods of subtropical gyre warming (i.e., Figure 3). Subtropical mode waters represent a subsurface reservoir of heat that extends south of the Gulf Stream extension. We find no similar interannual patterns of subsurface heat content change north of the Gulf Stream extension. Our interpretation of these results is consistent with past studies that attribute coastal sea level change to winds and Gulf Stream transport, and adds physical understanding to the connectivity of some location on the coast to a region offshore. This connectivity can thus be expected across all timescales of density variability at depths greater than the continental shelf break.

In this work we focus on only one process relevant to the coastal sea level budget. At the global scale, contributions to sea level rise from ice-sheet melt and ocean warming are roughly equal, but patterns of regional sea level change are the result of some combination of anthropogenically driven and inherent sterodynamic variability (Dangendorf et al., 2021; Hamlington et al., 2022). These sterodynamic changes reflect concurrent circulation change and mass redistribution, and shape where and how coastal regions are impacted. Results likewise have implications for projected regional sea level rise and variability changes due to ocean warming (Widlansky et al., 2020; Zhang et al., 2024), offering a mechanism to connect offshore to coastal variability. This study demonstrates the application of a framework by which these sterodynamic changes can be quantified along with any coastal response. From a prediction standpoint, the subannual to interannual explanatory power of this mass redistribution model suggests that subtropical North Atlantic heat content can serve as an important metric to monitor in anticipating future sea level changes across these timescales, a conclusion similar to the connection made by Widlansky et al. (2023) relating sea level and upper ocean temperature. These results also highlight the importance of resolving shelf-slope bathymetry in ocean simulations such that open-ocean changes can be realistically communicated to the coast.

Data Availability Statement

Tide gauge measurements of U.S. East Coast sea level were downloaded from the Permanent Service for Mean Sea Level (PSMSL, 2023). Rates of vertical land motion and surface pressure forcing were obtained at the Nevada Geodectic Library [http://geodesy.unr.edu/vlm.php] (Hammond et al., 2021) and the Copernicus Climate Data Store [https://cds.climate.copernicus.eu/#!/home] (Hersbach et al., 2020), respectively. NOAA GFDL NWA12 model output used in this analysis can be found on Zenodo [https://doi.org/10.5281/zenodo.7893387] (Ross et al., 2023).

Acknowledgments
Funding for this project was provided by the Bipartisan Infrastructure Law (BIL). We also acknowledge funding by NOAA's Climate Program Office and the NOAA Climate, Ecosystems, and Fisheries Initiative for NWA12 development. This work would not have been possible without the help and input from GFDL's MED division led by Charles Stock and the regional MOM6 development community. C.G.P. was supported by the NASA Sea Level Change Team (Grants 80NSSC20K1241 and 80NM0018D0004) and the Ocean Surface Topography Science Team (JPL subcontract 1670515). We thank Liping Zhang and Charles Stock at GFDL for comments on an early draft, as well as the editor and two anonymous reviewers for their thoughtful comments, all of which greatly helped improve this manuscript.

References

Alfieri, L., Lorini, V., Hirpa, F. A., Harrigan, S., Zsoter, E., Prudhomme, C., & Salamon, P. (2020). Global stream-flow reanalysis for 1980-2018. *Journal of Hydrology*, *6*, 100049. https://doi.org/10.1016/j.hydroa.2019.100049

Bingham, R. J., & Hughes, C. W. (2012). Local diagnostics to estimate density induced sea-level variations over topography and along coastlines. *Journal of Geophysical Research*, *117*(C1). https://doi.org/10.1029/2011JC007276

Calafat, F. M., Wahl, T., Lindsten, F., Williams, J., & Frajka-Williams, E. (2018). Coherent modulation of the sea-level annual cycle in the United States by atlantic rossby waves. *Nature Communications*, *9*(1), 2571. https://doi.org/10.1038/s41467-018-04898-y

Cazenave, A., & Moreira, L. (2022). Contemporary sea-Level changes from global to local scales: A review. *Proceedings of the Royal Society*, *478*(2261). https://doi.org/10.1098/rspa.2022.0049

Chassignet, E. P., & Marshall, D. P. (2008). Gulf stream separation in numerical ocean models. *Geophysical Monograph Series*, 39–61. https://doi.org/10.1029/177GM05

Chen, J., Tapley, B., Sea, K.-W., Wilson, C., & Ries, J. (2019). Improved quantification of global mean ocean mass change using grace satellite gravimetry measurements. *Geophysical Research Letters*, *46*(23), 13984–13991. https://doi.org/10.1029/2019GL085519

Chi, L., Wolfe, C. L. P., & Hameed, S. (2023). Reconsidering the relationship between gulf stream transport and dynamic sea level at u.s. east coast. *Geophysical Research Letters*, *50*(9). https://doi.org/10.1029/2022GL102018

Csanady, G. T. (1979). The pressure field along the western margin of the north atlantic. *Journal of Geophysical Research*, *84*(C8), 4905–4915. https://doi.org/10.1029/JC084iC08p04905

Dangendorf, S., Frederikse, T., Chafik, L., Klinck, J. M., Ezer, T., & Hamlington, B. (2021). Data-driven reconstruction reveals large-scale ocean circulation control on coastal sea level. *Nature Climate Change*, *11*(6), 514–520. https://doi.org/10.1038/s41558-021-01046-1

Dangendorf, S., Hendricks, N., Sun, Q., Klinck, J., Ezer, T., Frederikse, T., et al. (2023). Acceleration of u.s. southeast and gulf coast sea-level rise amplified by internal climate variability. *Nature Communications*, *14*(1), 1935. https://doi.org/10.1038/s41467-023-37649-9

Domingues, R., Goni, G., Baringer, M., & Volkov, D. (2018). What caused the accelerated sea level changes along the u.s. east coast during 2010-2015? *Geophysical Research Letters*, *45*(24). https://doi.org/10.1029/2018GL081183

Dong, S., Baringer, M. O., & Goni, G. J. (2019). Slow down of the gulf stream during 2013-2016. *Scientific Reports*, *9*(1), 6672. https://doi.org/10.1038/s41598-019-42820-8

Dusek, G., Sweet, W. V., Widlanksky, M. J., Thompson, P. R., & Marra, J. J. (2022). A novel statistical approach to predict seasonal high tide flooding. *Frontiers in Marine Science*, *9*. https://doi.org/10.3389/fmars.2022.1073792

Egbert, G. D., & Erofeeva, S. Y. (2020). Efficient inverse modeling of barotropic ocean tides. *Journal of Atmospheric and Oceanic Technology*, *19*(2), 183–204. https://doi.org/10.1175/1520-0426(2002)019⟨0183:EIMOBO⟩2.0.CO;2

Ezer, T. (2019). Regional differences in sea level rise between the mid-atlantic bight and the south atlantic bight: Is the gulf stream to blame? *Earth's Future*, *7*(7), 771–783. https://doi.org/10.1029/2019EF001174

Ezer, T., Atkinson, L. P., Corlett, W. B., & Blanco, J. L. (2013). Gulf stream's induced sea level rise and variability along the u.s. mid-atlantic coast. *Journal of Geophysical Research: Oceans*, *118*(2), 685–697. https://doi.org/10.1002/jgrc.20091

Ezer, T., & Dangendorf, S. (2020). Global sea level reconstruction for 1900-2015 reveals regional variability in ocean dynamics and an unprecedented long weakening in the gulf stream flow since the 1990s. *Ocean Science*, *16*(4), 997–1016. https://doi.org/10.5194/os-16-997-2020

Feng, X., Widlansky, M., Balmaseda, M., Zuo, H., Spillman, C., Smith, G., et al. (2024). Improved capabilities of global ocean reanalyses for analysing sea level variability near the atlantic and gulf of Mexico coastal u. s. *Frontiers in Marine Science*, *11*. https://doi.org/10.3389/fmars.2024.1338626

Forget, G., & Ponte, R. M. (2015). The partition of regional sea level variability. *Progress in Oceanography*, *137*, 173–195. https://doi.org/10.1016/j.pocean.2015.06.002

Fox-Kemper, B., Adcroft, A., Boning, C. W., Chassignet, E. P., Churchitser, E., Danabasoglu, G., et al. (2019). Challenges and prospects in ocean circulation models. *Frontiers in Marine Science*, *6*. https://doi.org/10.3389/fmars.2019.00065

Frederikse, T., Landerer, F., Caron, L., Adhikari, S., Parkes, D., Humphrey, V. W., et al. (2020). The causes of sea-level rise since 1900. *Nature*, *584*(7821), 393–397. https://doi.org/10.1038/s41586-020-2591-3

Frederikse, T., Lee, T., Wang, O., Kirtman, B., Becker, E., Hamlington, B., et al. (2022). A hybrid dynamical approach for seasonal prediction of seasea-level anomalies: A pilot study for charleston, South Carolina. *Journal of Geophysical Research: Oceans*, *127*(8). https://doi.org/10.1029/2021JC018137

Gan, B., Yu, J., Wu, L., Danabasoglu, G., Small, R. J., Baker, A. H., et al. (2023). North atlantic subtropical mode water formation controlled by gulf stream fronts. *National Science Review*, *10*(9). https://doi.org/10.1093/nsr/nwad133

Greatbatch, R. J. (1994). A note on the representation of steric sea level in models that conserve volume rather than mass. *Journal of Geophysical Research*, *99*(C6), 12767–12771. https://doi.org/10.1029/94JC00847

Griffies, S. M., & Greatbatch, R. J. (2012). Physical processes that impact the evolution of global mean sea level in ocean climate models. *Ocean Modelling*, *51*, 37–72. https://doi.org/10.1016/j.ocemod.2012.04.003

Griffies, S. M., Yin, J., Durack, P. J., Goddard, P., Bates, S. C., Behrens, E., et al. (2014). As assessment of global and regional sea level for years 1993-2007 in a suite of interannual core-ii simulations. *Ocean Modelling*, *78*, 35–89. https://doi.org/10.1016/j.ocemod.2014.03.004

Hamlington, B. D., Chambers, D. P., Frederikse, T., Dangendorf, S., Fournier, S., Buzzanga, B., & Nerem, S. (2022). Observations-based trajectory of future sea level for the coastal United States tracks near high-end model projections. *Communications Earth and Environment*, *3*(1), 230. https://doi.org/10.1038/s43247-022-00537-z

Hammond, W. C., Blewitt, G., Kreemer, C., & Nerem, R. S. (2021). Gps imaging of global vertical land motion for studies of sea level rise. *Journal of Geophysical Research: Solid Earth*, *126*(7). https://doi.org/10.1029/2021JB022355

Harvey, T. C., Hamlington, B. D., Frederikse, T., Nerem, R. S., Piecuch, C. G., Hammond, W. C., et al. (2021). Ocean mass, sterodynamic effects, and vertical land motion largely explain us coast relative sea level rise. *Communications: Earth and Environment*, *2*(1), 233. https://doi.org/10.1038/s43247-021-00300-w

Helland-Hansen, B. (1934). The sognefjord section: Oceanographic observations in the northernmost part of the north sea and the southern part of the Norwegian sea. *James Johnstong Memorial Volume*. https://doi.org/10.1029/JC084iC08p04905

Hersbach, H., Bell, B., Berrisford, P., Biavati, G., Horanyi, A., Munoz Sabater, J., et al. (2023). Era5 monthly averaged data on pressure levels from 1940 to present. *Copernicus Climate Change Service Climate Data Store*. [dataset]. https://doi.org/10.24381/cds.6860a573. accessed on 26 05 2022.

Hersbach, H., Bell, B., Berrisford, P., Hirahara, S., Horányi, A., Muñoz-Sabater, J., et al. (2020). Era5 global reanalysis. *Q.J. Royal Meteorological Society.*, *146*(730), 1999–2049. https://doi.org/10.1002/qj.3803

Higginson, S., Thompson, K. R., Woodworth, P. L., & Hughes, C. W. (2015). The tilt of mean sea level along the east coast of north America. *Geophysical Research Letters*, *42*(5), 1471–1479. https://doi.org/10.1002/2015GL063186

Hogarth, P. (2014). Preliminary analysis of acceleration of sea level rise through the twentieth century using extended tide gauge data sets (august 2014). *Journal of Geophysical Research: Oceans*, *119*(11), 7645–7659. https://doi.org/10.1002/2014JC009976

Hughes, C. W., Fukumori, I., Griffies, S. M., Huthnance, J. M., Minobe, S., Spence, P., et al. (2019). Sea level and the role of coastal trapped waves in mediating the influence of the open ocean on the coast. *Surveys in Geophysics*, *40*(6), 1467–1492. https://doi.org/10.1007/s10712-019-09535-x

Jevrejeva, S., Calafat, F., Dominicis, M., Hirschi, J., Mecking, J., Polton, J., et al. (2024). Challenges, advances and opportunities in regional sea level projections: The role of ocean-shelf dynamics. *Earth's Future*, *12*(8). https://doi.org/10.1029/2024EF004886

Johnson, G. C., & Lyman, J. M. (2020). Warming trends increasingly dominate global ocean. *Nature Climate Change*, *10*(8), 757–761. https://doi.org/10.1038/s41558-020-0822-0

Kolker, A. S., Allison, M. A., & Hameed, S. (2011). An evaluation of subsidence rates and sea-level variability in the northern gulf of Mexico. *Geophysical Research Letters*, *38*(21). https://doi.org/10.1029/2011GL049458

Kwon, Y.-O., & Riser, S. C. (2004). North atlantic subtropical mode water: A history of ocean-atmosphere interaction 1961–2000. *Geophysical Research Letters*, *31*(19). https://doi.org/10.1029/2004GL021116

Landerer, F. W., Jungclaus, J. H., & Marotzke, J. (2007). Ocean bottom pressure changes lead to a decreasing length-of-day in a warming climate. *Geophysical Research Letters*, *34*(6). https://doi.org/10.1029/2006GL029106

Lellouche, J.-M., Greiner, E., Bourdalle-Badie, R., Garric, G., Melet, A., Drevilon, M., et al. (2021). The copernicus global 1/12° oceanic and sea ice glorys12 reanalysis. *Frontiers in Earth Science*, *9*. https://doi.org/10.3389/feart.2021.698876

Li, D., Chang, P., Yeager, S. G., Danabasoglu, G., Castruccio, F. S., Small, J., et al. (2022). The impact of horizontal resolution on projected sea-level rise along us east continental self with the community earth system model. *Journal of Advances in Modeling Earth Systems*, *14*(5). https://doi.org/10.1029/2021MS002868

Li, Z., England, M. H., & Groeskamp, S. (2023). Recent acceleration in global ocean heat accumulation by mode and intermediate waters. *Nature Communications*, *14*(1), 6888. https://doi.org/10.1038/s41467-023-42468-z

Little, C. M., Hu, A., Hughes, C. W., McCarthy, G. D., Piecuch, C. G., Ponte, R. M., & Thomas, M. D. (2019). The relationship between u.s. East Coast sea level and the atlantic meridional overturning circulation: A review. *Journal of Geophysical Research: Oceans*, *124*(9), 6435–6458. https://doi.org/10.1029/2019JC015152

Liu, Y., Fasullo, J., & Galloway, D. L. (2020). Land subsidence contributions to relative sea level rise at tide gauge galveston pier 21, Texas. *Scientific Reports*, *10*(1), 17905. https://doi.org/10.1038/s41598-020-74696-4

Long, X., Widlansky, M., Spillman, C., Kumar, A., Balmaseda, M., Thompson, P., et al. (2021). Seasonal forecasting skill of sea-level anomalies in a multi-model prediction framework. *Journal of Geophysical Research: Oceans*, *126*(6). https://doi.org/10.1029/2020JC017060
Martinez-Moreno, J., Hogg, A., England, M. H., Constantinou, N. C., Kiss, A. E., & Morrison, A. K. (2021). Global changes in oceanic mesoscale currents over the satellite altimetry record. *Nature Climate Change*, *11*(5), 397–403. https://doi.org/10.1038/s41558-021-01006-9
McWilliams, J. C., Molemaker, J., & Damien, P. (2024). Baroclinic sea level. *Journal of Advances in Modeling Earth Systems*, *16*(4). https://doi.org/10.1029/2023MS003977
Minobe, S., Terada, M., Qiu, B., & Schneider, N. (2017). Western boundary sea level: A theory, rule of thumb, and application to climate models. *Journal of Physical Oceanography*, *47*(5), 957–977. https://doi.org/10.1175/JPO-D-16-0144.1
Nicholls, R. J. (2015). Planning for the impacts of sea level rise. *Oceanography*, *24*(2), 144–157. https://doi.org/10.5670/oceanog.2011.34
Nicholls, R. J., Lincke, D., Hinkel, J., Brown, S., Vafeidis, A., Meyssignac, B., et al. (2021). A global analysis of subsidence, relative sea-level change and coastal flood exposure. *Nature Climate Change*, *11*(4), 338–342. https://doi.org/10.1038/s41558-021-00993-z
Perez-Hernandez, M. D., & Joyce, T. M. (2014). Two modes of gulf stream variability revealed in the last two decades of satellite altimeter data. *Journal of Physical Oceanography*, *44*(1), 149–163. https://doi.org/10.1175/JPO-D-13-0136.1
PSMSL. (2023). Rlr monthly tide gauge data. *Permanent Service for Mean Sea Level*. [dataset] Retrieved from http://www.psmsl.org/data/obtaining. accessed on 28 03 2022.
Reid, J., & Mantyla, A. W. (1976). The effect of the geostrophic flod upon coastal sea elevations in the northern pacific ocean. *Journal of Geophysical Research*, *81*(18), 3100–3110. https://doi.org/10.1029/JC081i018p03100
Roemmich, D., & Gilson, J. (2009). The 2004-2008 mean annual cycle of temperature, salinity, and steric height in the global ocean from the argo program. *Progress in Oceanography*, *82*(2), 81–100. https://doi.org/10.1016/j.pocean.2009.03.004
Ross, A. C., Stock, C. A., Adcroft, A., Churchitser, E., Hallberg, R., Harrison, M. J., et al. (2023). A high-resolution physical-biogeochemical model for marine resource applications in the northwest atlantic (mom6-cobalt-nwa12 v1.0). *Geoscientific Model Development*, *16*(23), 6943–6985. https://doi.org/10.5194/gmd-16-6943-2023
Steinberg, J. M., Piecuch, C. G., Hamlington, B. D., Thompson, P. R., & Coats, S. (2024). Influence of deep-ocean warming coastal sea-level decadal trends in the gulf of Mexico. *Journal of Geophysical Research: Oceans*, *129*(1). https://doi.org/10.1029/2023JC019681
Stevens, S. W., Johnson, R. J., Maze, G., & Bates, N. (2020). A recent decline in north atlantic subtropical mode water formation. *Nature Climate Change*, *10*(4), 335–341. https://doi.org/10.1038/s41558-020-0722-3
Sun, Q., Dangendorf, S., Wahl, T., & Thompson, P. (2023). Causes of accelerated high-tide flooding in the u.s. since 1950. *NPJ Climate and Atmospheric Science*, *6*(1), 210. https://doi.org/10.1038/s41612-023-00538-5
Sweet, W. V., Genz, A., Menendez, M., Marra, J., & Obeysekera, J. (2024). Implications of variability and trends in coastal extreme water levels. *Geophysical Research Letters*, *51*(14). https://doi.org/10.1029/2024GL108864
Sweet, W. V., Hamlington, B. D., Kopp, R. E., Weaver, C. P., Barnard, P. L., Bekaert, D., et al. (2022). *Global and regional sea level rise scenarios for the United States: Up-dated mean projections and extreme water level probabilities along u.s. coastlines. NOAA Technical Report NOS 01*. National Oceanic and Atmospheric Administration, National Ocean Service, Silver Spring.
Talke, S. A., Kemp, A. C., & Woodruff, J. (2018). Relative sea level, tides, and extreme water levels in boston harbor from 1825 to 2018. *Journal of Geophysical Research: Oceans*, *123*(6), 3895–3914. https://doi.org/10.1029/2017JC013645
Thirion, G., Birol, F., & Jouanno, J. (2024). Loop current eddies as a possible cause of the rapid sea level rise in the gulf of Mexico. *Journal of Geophysical Research: Oceans*, *129*(3). https://doi.org/10.1029/2023JC019764
Thompson, P. R., & Mitchum, G. T. (2014). Coherent sea level variability on the north atlantic western boundary. *JGR: Oceans*, *119*(9), 5676–5689. https://doi.org/10.1002/2014JC009999
Todd, R. E., & Ren, A. S. (2023). Warming and lateral shift of the gulf stream from in situ observations since 2001. *Nature Climate Change*, *13*(12), 1348–1352. https://doi.org/10.1038/s41558-023-01835-w
Vignudelli, S., Birol, F. J. B., Fu, L. L., Picot, N., Raynal, M., & Roinard, H. (2019). Satellite altimetry measurements of sea level in the coastal zone. *Surveys in Geophysics*, *40*(6), 1319–1349. https://doi.org/10.1007/s10712-019-09569-1
Vinogradova, N. T., Ponte, R. M., & Stammer, D. (2007). Relation between sea level and bottom pressure and the vertical dependence of oceanic variability. *Geophysical Research Letters*, *34*(3). https://doi.org/10.1029/2006GL028588
Volkov, D. L., Lee, S. K., Domingues, R., Zhang, H., & Goes, M. (2019). Interannual sea level variability along the southeastern seaboard of the United States in relation to the gyre-scale heat divergence in the north atlantic. *Geophysical Research Letters*, *46*(13), 7481–7490. https://doi.org/10.1029/2019GL083596
Volkov, D. L., Zhang, K., Johns, W. E., Willis, J. K., Hobbs, W., Goes, M., et al. (2023). Atlantic meridional overturning circulation increases flood risk along the United States southeast coast. *Nature Communications*, *14*(1), 5095. https://doi.org/10.1038/s41467-023-40848-z
Wang, O., Lee, T., Frederikse, T., Ponte, R., Fenty, I., Fukumori, I., & Hamlington, B. D. (2024). What forcing mechanisms affect the interannual sea level co-variability between the northeast and southeast coasts of the United States? *Journal of Geophysical Research: Oceans*, *129*(1). https://doi.org/10.1029/2023JC019873
Wang, O., Lee, T., Piecuch, C. G., Fukumori, I., Fenty, I., Frederikse, T., et al. (2022). Local and remote forcing of interannual sea-level variability at nantucket. *Journal of Geophysical Research: Oceans*, *127*(6). https://doi.org/10.1029/2021JC018275
Widlansky, M., Long, X., Balmaseda, M., Spillman, C., Smith, G., Zuo, H., et al. (2023). Quantifying the benefits of altimetry assimilation in seasonal forecasts of the upper ocean. *Journal of Geophysical Research: Oceans*, *128*(5). https://doi.org/10.1029/2022JC019342
Widlansky, M., Long, X., & Schlosser, F. (2020). Increase in sea level variability with ocean warming associated with the nonlinear thermal expansion of seawater. *Communications: Earth and Environment*, *1*(1), 9. https://doi.org/10.1038/s43247-020-0008-8
Wise, A., Hughes, C. W., & Polton, J. A. (2018). Bathymetric influence on the coastal sea level response to ocean gyres at western boundaries. *Journal of Physical Oceanography*, *48*(12), 2949–2964. https://doi.org/10.1175/JPO-D-18-0007.1
Wise, A., Hughes, C. W., Polton, J. A., & Huthnance, J. M. (2020a). Leaky slope waves and sea level: Unusual consequences of the beta effect along western boundaries with bottom topography and dissipation. *Journal of Physical Oceanography*, *50*(1), 217–237. https://doi.org/10.1175/JPO-D-19-0084.1
Wise, A., Polton, J. A., Hughes, C. W., & Huthnance, J. M. (2020b). Idealized modelling of offshore-forced sea level hot spots and boundary waves along the north american east coast. *Ocean Modelling*, *155*, 101706. https://doi.org/10.1016/j.ocemod.2020.101706
Woodworth, P. L., Melet, A., Marcos, M., Ray, R. D., Wöppelmann, G., Sasaki, Y. N., et al. (2019). Forcing factors affecting seat level changes at the coast. *Surveys in Geophysics*, *40*(6), 1351–1397. https://doi.org/10.1007/s10712-019-09531-1
Woodworth, P. L., Morales Maqueda, M. A., Gehrels, W. R., Roussenov, V. M., Williams, R. G., & Hughes, C. W. (2016). Variations in the difference between mean sea level measured either side of cape hatteras and their relation to the north atlantic oscillation. *Climate Dynamics*, *49*(7–8), 2451–2469. https://doi.org/10.1007/s00382-016-3464-1

Yin, J. (2023). Rapid decadal acceleration of sea level rise along the u.s. east and gulf coasts during 2010-2012 and its impact on hurricane-induced storm surge. *Journal of Climate*, *36*(13), 4511–4529. https://doi.org/10.1175/JCLID-22-0670.1

Yin, J., Griffies, S. M., & Stouffer, R. J. (2010). Spatial variability of sea level rise in twenty-first century projections. *Journal of Climate*, *23*(17), 4585–4607. https://doi.org/10.1175/2010JCLI3533.1

Zhang, L., Delworth, T. L., Yang, X., Zeng, F., Gu, Q., & Li, S. (2024). Causes and multiyear predictability of the rapid acceleration of u.s. southeast sea level rise after 2010. *npj Clim Atmos Sci*, *7*(1), 113. https://doi.org/10.1038/s41612-024-00670-w

Zika, J. D., Gregory, J. M., McDonagh, E. L., Marzocchi, A., & Clement, L. (2021). Recent water mass changes reveal mechanisms of ocean warming. *Journal of Climate*, *34*(9), 3461–3479. https://doi.org/10.1175/JCLI-D-20-0355.1